

Wide ultrarelativistic plasma-beam–magnetic-barrier collision

V. V. Usov and M. V. Smolsky

Department of Condensed Matter Physics, Weizmann Institute, Rehovot 76100, Israel

(Received 9 April 1997)

The interaction between a wide ultrarelativistic fully ionized plasma beam and a magnetic barrier is studied numerically. It is assumed that the plasma beam is initially homogeneous and impacts with the Lorentz factor $\Gamma_0 \gg 1$ on the barrier. The magnetic field of the barrier \mathbf{B}_0 is uniform and transverse to the beam velocity. When the energy densities of the beam and the magnetic field are comparable, $\alpha = 8\pi n_0 m_p c^2 (\Gamma_0 - 1) / B_0^2 \sim 1$, the process of the beam-barrier interaction is strongly nonstationary and the density of reversed protons is modulated in space by a factor of 10 or so. The modulation of reversed protons decreases with decrease of α . The beam is found to penetrate deep into the barrier provided that $\alpha > \alpha_{cr}$, where α_{cr} is about 0.4. The speed of such a penetration is subrelativistic and depends on α . Strong electric fields are generated near the front of the barrier and electrons are accelerated in these fields up to the mean energy of protons, i.e., up to $\sim m_p c^2 \Gamma_0$. The synchrotron radiation of high-energy electrons from the front vicinity is calculated. Stationary solutions for the beam-barrier collision are considered. It is shown that such a solution may be only at $\alpha \lesssim 0.2-0.5$, depending on the boundary conditions for the electric field in the region of the beam-barrier interaction. [S1063-651X(98)04602-9]

PACS number(s): 41.75.-i, 95.30.Gv, 95.85.Pw, 98.70.Rz

I. INTRODUCTION

There is now compelling evidence that plasma is ejected from many astronomical objects and flows away at relativistic speeds. The Lorentz factor Γ_0 of such plasma wind is a few $\times (1-10)$ for the jets associated with active galactic nuclei [1] and $\sim 10^2-10^3$ or even more for the γ -ray bursters [2]. A strong magnetic field may be in the outflowing gas [3-6]. Relativistic magnetized winds can interact with an external medium (e.g., an ordinary interstellar medium). It was pointed out in Ref. [7] that such an interaction may be responsible for radiation of both x rays and γ rays from the γ -ray bursters. For consideration of the interaction between a relativistic magnetized wind and an external medium, it is convenient to switch to the wind frame. In this frame, the problem of the magnetized wind–external medium interaction is identical to the problem of collision between a wide relativistic beam of cold plasma and a region with a strong magnetic field, which is called a magnetic barrier.

The problem of the interaction between plasma beams and magnetic barriers was attacked in many experiments and theoretical papers (see Ref. [8] and references therein). However, all known experimental studies of the beam–magnetic-barrier interaction are irrelevant to our problem. This is because the plasma beams produced by the laboratory equipment are either nonrelativistic or very narrow and the cross-beam sizes are much smaller than the gyroradius of the beam protons in the field of the barrier. In the theoretical studies, it is usually used the assumption of Rosenbluth [9] that the charge separation is small. However, this assumption is valid provided the inequality $(v_0/c)^2 \ll m_e/m_p \approx 5.4 \times 10^{-4}$ holds true, where v_0 is the beam velocity, m_e is the electron mass, and m_p is the proton mass. For relativistic beams, $v_0 = c\sqrt{1 - (1/\Gamma_0)^2} \approx c$, the assumption of Rosenbluth proves inadequate and the charge separation is very important for the dynamics of particles near the barrier front [10,11]. Below, the interaction of a wide ultrarelativistic plasma beam

with a magnetic barrier is considered numerically (for preliminary results and some astrophysical applications see Ref. [11]).

II. FORMULATION OF THE PROBLEM AND BASIC EQUATIONS

The situation to be discussed is the following. At the initial moment $t=0$ the ultrarelativistic (Lorentz factor $\Gamma_0 \gg 1$) neutral beam of protons and electrons (number densities $n_p = n_e \equiv n_0$) runs along the x axis into the magnetic barrier, which is the half space $x > 0$ with an external magnetic field $\mathbf{B}_0 = B_0 \hat{e}_z \Theta(x)$, where n_0, B_0 are constants and $\Theta(x)$ is the step function equal to unity for $x > 0$ and to zero for $x < 0$. The beam is infinite in the y - z dimensions and semi-infinite in the x dimension. Our goal is to construct a $1\frac{1}{2}$ dimensional time-dependent solution for the problem, i.e., to find induced electromagnetic fields ($\mathbf{E} = E_x \hat{e}_x + E_y \hat{e}_y$, $\mathbf{B} = B \hat{e}_z$) and motion of the beam particles in the x - y plane. The field structure and the beam particle motion are to be treated self-consistently. All the quantities are assumed to be dependent on t and x only.

As noted earlier, the strength of the magnetic fields in the astrophysical winds may be very high, especially in the winds flowing out from the γ -ray bursters [4,5]. High-energy electrons generate synchrotron radiation in these fields and the radiation damping force that acts on the radiating electrons has to be taken into account. Since $m_p \gg m_e$, both the synchrotron radiation of protons and the radiation damping force that acts on the protons are very small (e.g., Ref. [12]) and may be neglected.

The following set of equations can be used to describe the process of the beam–barrier collision [12]:

$$\frac{\partial E_x}{\partial x} = 4\pi\rho, \quad (1)$$

$$\frac{\partial E_y}{\partial x} = -\frac{1}{c} \frac{\partial B}{\partial t}, \quad (2)$$

$$\frac{\partial B}{\partial x} = -\frac{1}{c} \frac{\partial E_y}{\partial t} - \frac{4\pi}{c} j_y, \quad (3)$$

$$mc \frac{du^i}{ds} = \frac{e}{c} F^{ik} u_k + \frac{2e^4}{3m^2 c^5} (F_{kl} u^l) (F^{km} u_m) u^i, \quad (4)$$

where ρ and \mathbf{j} are the densities of charges and currents, respectively, e is the charge of particles, m is the mass of particles, $m = \{m_e, m_p\}$, s is the interval, $u^i = \{\Gamma, (\mathbf{v}/c)\Gamma\}$ is the four-velocity, Γ is the Lorentz factor of particles, and F^{ik} is the electromagnetic-field tensor. No simplifying assumptions besides geometrical ones are exploited when rewriting Maxwell equations (1)–(3). The second term on the right-hand side of the relativistic equation of particle motion (4) is the radiation damping four-force. Following Ref. [11], only the term of the highest power in Γ is left in the damping force. This is valid for ultrarelativistic motion of particles $\Gamma \gg 1$ (e.g., Ref. [12]).

The four-velocity u^i from Eq. (4) is related to the charge and current densities that appear in the Maxwell equations (1)–(3):

$$j^i = \{c\rho, j_x, j_y, 0\} = \sum c e \Gamma^{-1} u^i, \quad (5)$$

where Σ means the sum over the beam particles per unitary volume. The energy losses I of electrons because of their radiation in the electric and magnetic fields are computed using the equation [12]

$$I = \frac{2e^4}{3m_e^2 c^3} \left\{ \left(\mathbf{E} + \frac{1}{c} \mathbf{v} \times \mathbf{B} \right)^2 - \frac{1}{c^2} (\mathbf{E} \cdot \mathbf{v})^2 \right\} \Gamma^2. \quad (6)$$

To evaluate the spectrum of the radiation of electrons, we have used the following expression for the spectral intensity of synchrotron radiation [13]:

$$I_\nu = \frac{\sqrt{3} e^3 B}{m_e c^2} \frac{\nu}{\nu_c} \int_{\nu/\nu_c}^{\infty} K_{5/3}(\eta) d\eta, \quad (7)$$

where $K_{5/3}$ is the modified Bessel functions of 5/3 order,

$$\nu_c = \frac{3eB\Gamma^2}{4\pi m_e c}. \quad (8)$$

In Eqs. (7) and (8), it is taken into account that in our case the velocities of particles are perpendicular to the magnetic field $\mathbf{v} \perp \mathbf{B}$.

The initial beam number density is taken from the equation

$$n_0 m_p c^2 (\Gamma_0 - 1) = \alpha \frac{B_0^2}{8\pi}, \quad (9)$$

where α is the dimensionless parameter. In this work we study mainly the case $\alpha \sim 1$ when the plasma flow pressure is

TABLE I. Input parameters of simulations.

Run	B_0 (G)	Γ_0 (10^3)	α	$-x_{\min}$ (c/ω_{Bp})	x_{\max} (c/ω_{Bp})	t_{\max} (T_p)
A	100	0.1	2	5	10	2.8
B	300	0.3	2	5	10	2.8
C	300	1	2	5	12	3.3
D	10^4	0.5	2	5	7	3.3
E	10^4	1	2	10	7	3.5
F	10^4	2	2	5	5	2.4
G	10^5	1	2	10	5	2.3
H	10^4	1	1	10	5	4.4
I	10^3	1	4	5	20	3.5
J	10^4	1	0.2	5	15	5.1
K	300	0.3	1/3	10	5	10.6
L	300	0.3	2/5	10	5	10.6
M	300	0.3	4/7	5	30	10.6
N	300	0.3	2/3	5	30	15.9
O	300	0.3	1	5	30	10.6
P	300	0.3	2	5	30	10.6

comparable to the magnetic-field pressure of the barrier. In different runs, α ranges from 0.2 to 4.

To integrate the set of equations (1)–(9) we used a macroparticle approximation in which all particles of the beam are subdivided into a large number ($\sim 10^4$) of packets. The particles within a packet are bundled together forming a large macroparticle that is infinitively small along the axis x and infinitively large in all directions of the y - z plane. Each packet contains either protons or electrons (for details of the numerical method see Ref. [11]).

The examined space-time domain is

$$x_{\min} < x < x_{\max}, \quad 0 < t < t_{\max}, \quad (10)$$

where x_{\min} is equal to a few $\times (1-10)(c/\omega_{Bp})$, x_{\max} is equal to a few $\times (1-10)(c/\omega_{Bp})$, t_{\max} is equal to a few $\times (1-10) T_p$, $T_p = 2\pi/\omega_{Bp}$ is the proton gyroperiod, and $\omega_{Bp} = eB_0/m_p c \Gamma_0$ and $c/\omega_{Bp} = m_p c^2 \Gamma_0 / eB_0$ are the proton gyrofrequency and gyroradius, respectively. The time step of calculations is a few $\times 10^{-6} T_p$, depending on α .

The boundary condition for E_x is $E_x|_{x=x_{\max}} = 0$, as x_{\max} is chosen so that no beam particles penetrate deeper than x_{\max} in the observed interval of time. Electromagnetic waves generated due to charge flow are allowed to escape freely from the system that is used as boundary conditions for B and E_y in Eqs. (2) and (3).

III. RESULTS OF NUMERICAL SIMULATIONS AND SCALING

The relativistic cold plasma–magnetic-barrier collision is characterized by the following parameters: B_0 , Γ_0 , and α . The input parameters of our simulations are given in Table I. The values of B_0 and Γ_0 are chosen to be relevant to cosmological γ -ray bursters [3–5,7,11].

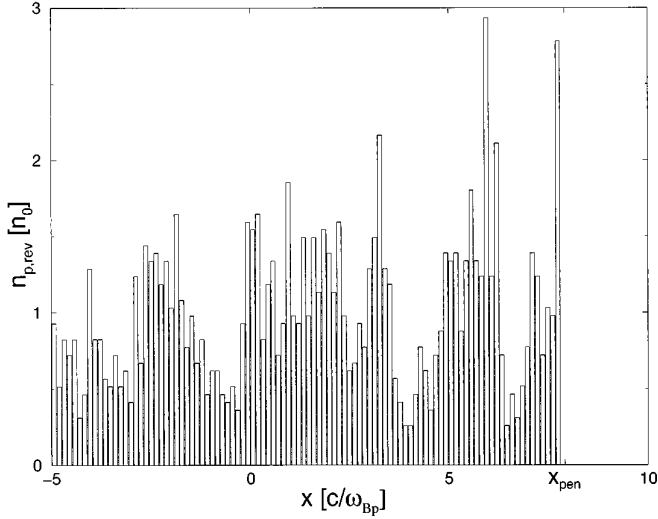


FIG. 1. Density of reversed protons in units of n_0 in run N.

A. Particle dynamics and penetration of the beam particles into the barrier

The density of protons that move towards the magnetic barrier ($v_x > 0$) is almost unperturbed until the distance to the barrier is smaller than $\sim c/\omega_{Bp}$. Reversed protons that move away from the magnetic barrier ($v_x < 0$) are bunched in the process of the beam-barrier interaction (Fig. 1). The modulation of the density of reversed protons is strong at $\alpha \sim 1$ and decreases with decrease of α . Namely, the ratio of the maximum to minimum densities of reversed protons is ~ 10 at $\alpha \approx 1$ and ~ 2 at $\alpha \approx 0.2$. A typical length of such a modulation is roughly the proton gyroradius c/ω_{Bp} . A similar phenomenon was observed also in numerical simulations of collisionless shock waves near the shock front (e.g., Ref. [14]).

At $\alpha \sim 1$, the mean Lorentz factor of reversed protons that are far enough from the barrier $x < -(c/\omega_{Bp})$, where the process of a strong interaction between particles and fields is more or less over, is $\langle \Gamma_p^{\text{out}} \rangle \approx (0.5 \pm 0.1)\Gamma_0$, i.e., about half of

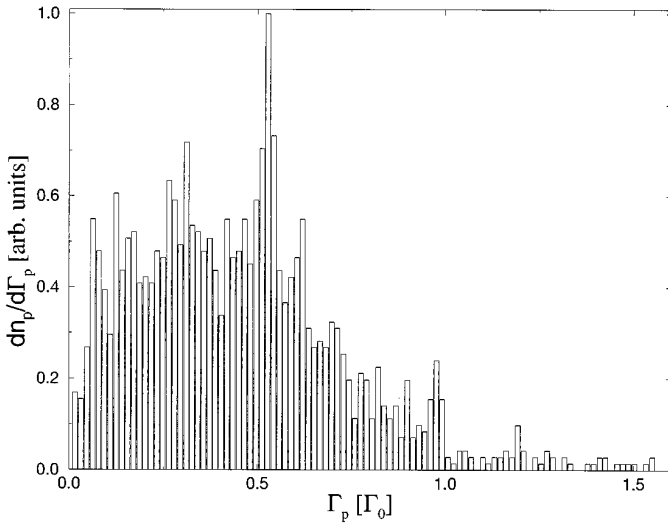


FIG. 2. Energy spectrum of reversed protons at $x < -(c/\omega_{Bp})$ in run N.

TABLE II. Derived parameters of simulations.

Run	$\frac{\langle \Gamma_e^{\text{out}} \rangle}{\Gamma_0}$	$\frac{\Gamma_{e,\text{max}}^{\text{out}}}{\Gamma_0}$	$\frac{\langle \Gamma_e^{\text{rad}} \rangle}{\Gamma_0}$	$\frac{\langle \Gamma_p^{\text{out}} \rangle}{\Gamma_0}$	ξ_γ (10^{-2})	$\langle \epsilon_\gamma \rangle$ MeV
A	132	603	643	0.61	3.2×10^{-3}	0.013
B	107	785	809	0.41	0.12	0.45
C	106	464	543	0.57	0.96	5.1
D	119	745	425	0.48	3.4	8.9
E	92	542	337	0.48	11	14
F	92	785	235	0.40	12	35
G	56	402	193	0.43	14	36
H	116	801	419	0.57	9.9	15
I	105	427	555	0.41	2.9	9.1
J	9.5	39	41	0.99	0.16	0.20
K	115	573	288	0.94	0.017	0.09
L	424	1473	596	0.73	0.052	0.19
M	296	1038	913	0.69	0.18	0.64
N	489	1275	807	0.50	0.36	0.34
O	213	1284	821	0.62	0.16	0.34
P	94	550	883	0.63	0.42	0.68

the initial kinetic energy of protons, is lost in the process of their collision with the barrier (see Table II). Figure 2 shows the energy distribution for reversed protons.

The density of electrons that move away from the barrier is well correlated with the density of reversed protons; the correlation coefficient is $r \approx 0.8$, where $r = \sigma_{pe} / \sqrt{\sigma_{pp}\sigma_{ee}}$, and

$$\sigma_{ij} = \int_{x_{\text{min}}}^{x_{\text{max}}} (n_i - \bar{n}_i)(n_j - \bar{n}_j) dx, \quad \{i, j\} = \{e, p\}. \quad (11)$$

These electrons screen the electrostatic field E_x of proton bunches mostly, but not completely.

At $\alpha > \alpha_{\text{cr}}$, $\alpha_{\text{cr}} \approx 0.4$, it is observed that the length of the beam particle penetration into the barrier increases in time. Figure 3 shows the x coordinate x_{pen} of the most deeply penetrated proton as a function of time t . The speeds of such

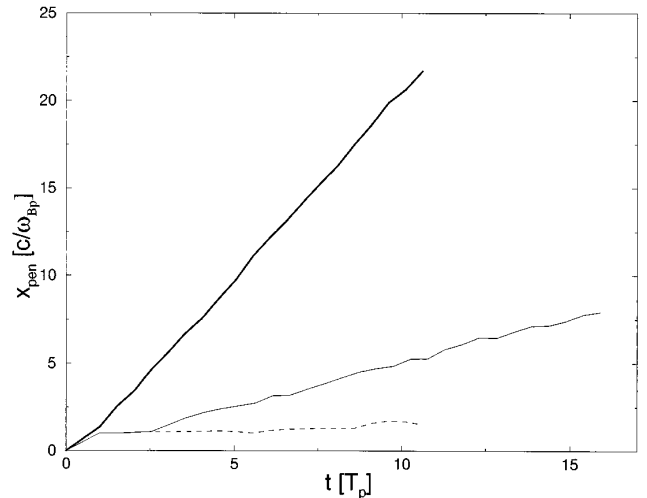


FIG. 3. Beam penetration depth x_{pen} as a function of time t in run P (thick solid line), in run N (thin solid line), and in run L (dotted line).

TABLE III. Penetration of the beam particles with $\Gamma_0=300$ into the magnetic barrier with $B_0=300$ G for different values of α .

α	2	1	2/3	4/9	2/5	1/3
v_{pen}/c	0.32	0.17	0.077	0.05	0	0

protons along the x axis vary strongly from each other. However, the mean velocity $v_{\text{pen}}=\langle v_x \rangle$ of the penetrated protons remains more or less constant within the studied time intervals, where $\langle v_x \rangle$ is the proton velocity that is averaged over proton gyroperiod. The value of v_{pen} depends on α and is equal to zero (no penetration) at $\alpha < \alpha_{\text{cr}} \approx 0.4$ (see Fig. 3 and Table III).

In the region $x < x_{\text{pen}}$, strong longitudinal (E_x) and transverse (E_y, B_z) electromagnetic waves propagate while almost no remnants of the external magnetic field $B_0 \Theta(x)$ are found (Fig. 4). Roughly, it could be stated that at $\alpha > \alpha_{\text{cr}}$ the magnetic barrier is pushed according to the law $B(t) = B_0 \Theta(x - x_{\text{pen}}(t))$ and x_{pen} appears to be a location of the barrier front at the moment t as well as the particle penetration depth. At $x > x_{\text{pen}}$, the magnetic field remains unchanged except for its time-space variations due to low-frequency electromagnetic waves that are generated by the time-variable currents \mathbf{j} in the front vicinity. At $\alpha \sim 1$, the typical amplitude of these waves is $\tilde{B}_0 \approx (0.2-0.3)B_0$.

In the case $\alpha < \alpha_{\text{cr}}$, when the ion penetration length does not increase with time, all protons move along the same track with small deviations from it. In this case, the velocity of all reversed protons is perpendicular to the barrier front. However, at $\alpha > \alpha_{\text{cr}}$ the trajectories of protons differ qualitatively from each other (for the angular distribution of reversed protons in this case see Fig. 5). Therefore, the dimensionless density α may be called a stochastization parameter of the beam protons. In all runs, the trajectories of electrons are very chaotic and differ from each other qualitatively.

B. Acceleration of electrons and high-frequency radiation

The most important feature of the dynamics of electrons is that they are accelerated in the barrier front vicinity by

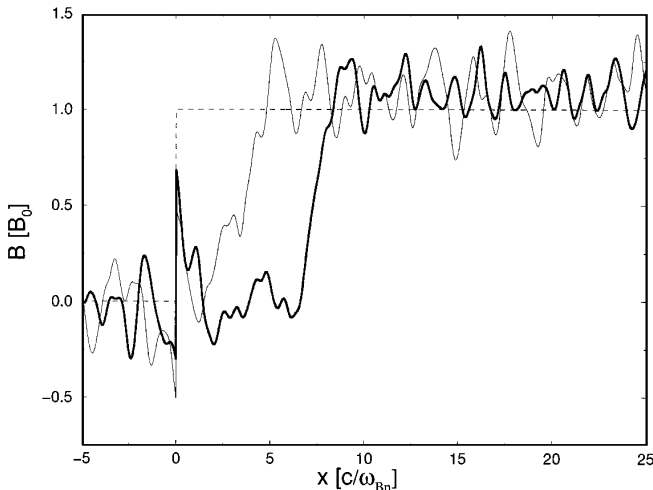


FIG. 4. Distribution of magnetic field in run N at the moments $t=0$ (dotted line), $t=7.96T_p$ (thin solid line), and $t=15.9T_p$ (thick solid line).

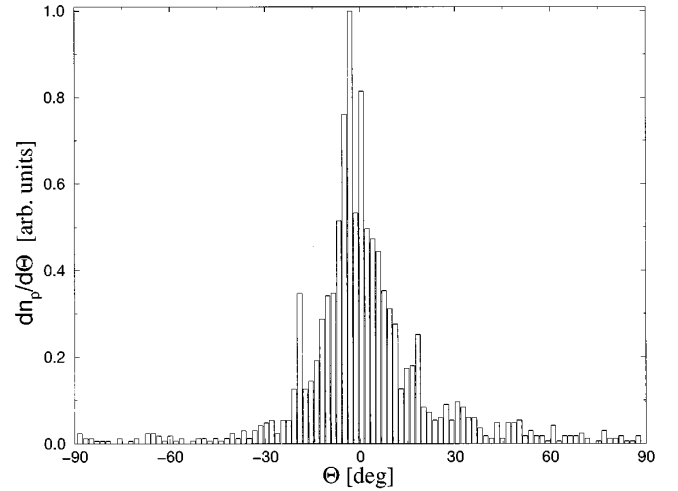


FIG. 5. Angular distribution of reversed protons at $x < -(c/\omega_{Bp})$ in run N.

induced electric fields and thus accumulate a substantial portion of the kinetic energy of protons (see Fig. 6 and Table II). Figure 7 shows the energy spectrum of outflowing electrons, $v_x < 0$, in run N. At $\alpha \sim 1$, the mean Lorentz factor of outflowing electrons and their maximum Lorentz factor far enough from the barrier $x < -(c/\omega_{Bp})$ are

$$\langle \Gamma_e^{\text{out}} \rangle \approx 0.1 \left(\frac{m_p}{m_e} \right) \Gamma_0, \quad \Gamma_{e,\text{max}}^{\text{out}} \approx \frac{1}{2} \left(\frac{m_p}{m_e} \right) \Gamma_0 \quad (12)$$

within a factor of 2. The fraction of the kinetic energy of relativistic protons that is transformed into the energy of outflowing electrons is up to $\sim 20\%$. The rest of the energy that is lost by protons is transformed into both low-frequency electromagnetic waves and synchrotron high-frequency radiation.

The synchrotron high-frequency radiation is generated by single electrons in the process of their ultrarelativistic motion in the electromagnetic fields. The mean energy of so-called radiating electrons near the barrier front $x > -(c/\omega_{Bp})$ is several times higher than the mean energy of outflowing electrons far from the barrier $x < -(c/\omega_{Bp})$, i.e., $\langle \Gamma_e^{\text{rad}} \rangle \approx (3-5) \langle \Gamma_e^{\text{out}} \rangle$ (see Table II). The radiating electrons

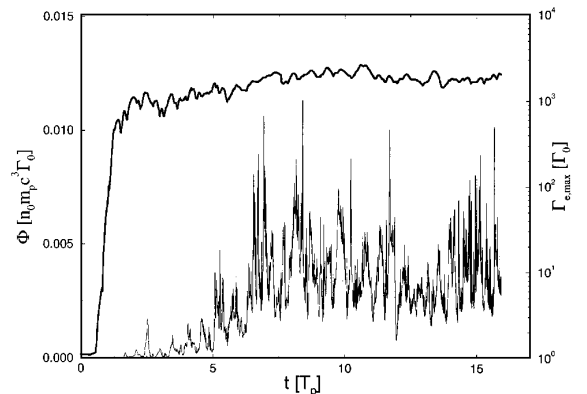


FIG. 6. Maximum energy of accelerated electrons (thick line) and intensity of their synchrotron radiation per unitary area of the barrier front (thin line) in run N.

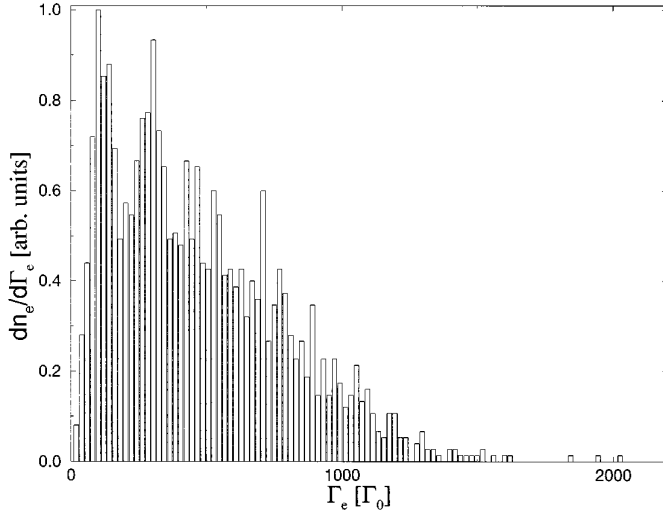


FIG. 7. Energy spectrum of outflowing electrons, $v_x < 0$, in run N at the moment $t = 15.9T_p$.

are responsible for generation of the main part of the synchrotron high-frequency emission.

If the average fraction ξ_γ of the kinetic energy of the plasma beam that is radiated in the vicinity of the magnetic barrier is small, $\xi_\gamma < 0.01$ or $\Gamma_0^2 B_0 < 3 \times 10^8$ G, the results of our simulations for $\alpha \sim 1$ may be fitted by the analytic expression

$$\xi_\gamma \approx 3 \times 10^{-4} (\Gamma_0/10^2)^2 [B_0/(10^3 \text{G})]. \quad (13)$$

At $\Gamma_0^2 B_0 \gg 10^8$ G, the value of ξ_γ tends asymptotically to ~ 0.15 as $\Gamma_0^2 B_0$ increases. The characteristic energy of synchrotron photons is

$$\langle \varepsilon_\gamma \rangle \approx 3 (\xi_\gamma / 10^{-2}) \text{ MeV} \quad (14)$$

within a factor of 2 or so. Except for numerical factors, Eqs. (13) and (14) can be derived analytically from Eqs. (1)–(9).

At $\alpha \ll 1$, electromagnetic fields that are induced in the process of the beam-barrier collision are much smaller than B_0 and the beam particles may be treated as test particles in the field of the barrier. In this case, there is almost no energy transfer from protons to electrons. Therefore, it is natural that both acceleration of electrons and their high-frequency radiation are strongly suppressed at $\alpha \ll 1$, as was observed in our simulations (see Table II). Preliminarily, we have the following scaling laws: $\langle \Gamma_e^{\text{out}} \rangle \propto \alpha$, $\Gamma_{e,\text{max}}^{\text{out}} \propto \alpha$, $\langle \Gamma_e^{\text{rad}} \rangle \propto \alpha$, $\xi_\gamma \propto \alpha^2$, and $\langle \varepsilon_\gamma \rangle \propto \alpha^2$. We did not observe any decrease in nonstationarity of the process of the beam-barrier interaction and in acceleration of electrons, even in simulations extended up to $t_{\text{max}} \approx 16T_p$ (see Figs. 1 and 6).

IV. STATIONARY COLLISION

The problem of the beam-barrier collision is simplified significantly if it is treated as a stationary one. This is because in a stationary consideration a time dependence of all values is disregarded and the beam particles of any kind (protons or electrons) move along exactly the same track. In this section we consider the beam-barrier interaction in a stationary manner.

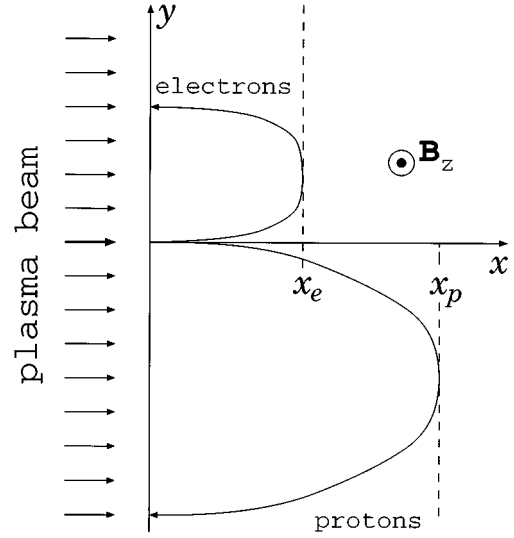


FIG. 8. Schematic drawing of a plasma beam entering a magnetic barrier.

A fully relativistic self-consistent model of the stationary interaction between a wide plasma beam and a magnetic barrier was developed by Peter, Ron, and Rostocker in their pioneering paper [10]. The set of equations that describes such an interaction is [10]

$$\frac{dB_z}{dx} = A_y \left(\frac{m_e/m_p}{\sqrt{z_p}} + \frac{1}{\sqrt{z_e}} \right), \quad (15)$$

$$\frac{dE_x}{dx} = \frac{\Gamma_p}{\sqrt{z_p}} - \frac{\Gamma_e}{\sqrt{z_e}}, \quad (16)$$

$$\frac{d\phi}{dx} = -E_x, \quad \frac{dA_y}{dx} = B_z, \quad (17)$$

where $\Gamma_j \equiv \Gamma_0 - \mu_j \phi$, $z_j \equiv \Gamma_j^2 - \mu_j^2 A_y^2 - 1$,

$$\mu_j \equiv \begin{cases} -1 & \text{for electrons } (j=e) \\ m_e/m_p & \text{for protons } (j=p), \end{cases} \quad (18)$$

ϕ and A_y are the electrostatic and magnetic potentials in units of e/mc^2 . In these equations we have measured the distance x in terms of $\sqrt{2}(\omega_{pe}\beta_0/c)$, where $\omega_{pe} = (4\pi n_0 e^2/m_e)^{1/2}$ is the electron plasma frequency and $\beta_0 = v_0/c$.

Equations (15) and (16) for the magnetic and electric fields are first-order ordinary differential equations. Strictly speaking, such an equation allows only one boundary condition. For the magnetic field B_z , the boundary condition is $B_z = B_0$ at the proton turning point x_p (see Fig. 8), where B_0 is the field of the barrier. The strength of the magnetic field B_f at the front of the barrier $x=0$ has to be found from integration of Eq. (15). An important issue is *where* the electric field E_x should vanish: at the right or left boundary of the collision region $0 \leq x \leq x_p$. In Ref. [10] the electric field vanishes at $x = x_p$, $E_x|_{x=x_p} = 0$. This seems quite natural and corresponds to our nonstationary solution. However, in Ref. [10] it is wrongly suggested that if the beam density is high

enough the electric field E_x is zero at the left boundary as well, $E_x|_{x=0}=0$. Below, stationary solutions for the beam-barrier collision are considered in detail and, in particular, it is shown that there is a net charge in the region $0 \leq x \leq x_p$ irrespective of the beam density until the beam-barrier collision is stationary, i.e., the transverse electric field E_x cannot be zero at both boundaries at once.

The right-hand side of Eqs. (15) and (16) for the derivatives of the electric and magnetic fields contains terms that tend to infinity at the electron and proton turning points, i.e., at both $x=x_e$ and $x=x_p$. This is the main difficulty that does not permit one to apply a standard numerical technique to integrate Eqs. (15) and (16) directly. Since the electric and magnetic fields should remain finite everywhere, the mentioned singularities are integrable. To integrate a set of equations with such a weak, integrable singularity, one should switch to another independent variable so that all derivatives with respect to this new variable are finite. The interval of the beam particles may be used as such a new independent variable instead of x . In this case, the right-hand sides of Eqs. (15) and (16) are finite everywhere. This is because the particle density per unitary interval is constant (e.g., Ref. [10]) rather than infinite at the turning points if measured per unitary x . We integrated Eqs. (15)–(17) from $x=0$ to $x=x_e$ using the *electron* interval s_e as an independent variable. Then we switched to another independent variable s_p , which is the *proton* interval measured from the *electron* turning point with the initial condition $s_p|_{x=x_e}=s_e|_{x=x_e}$. We thus broke the region of integration into two parts and used a different independent variable for each subinterval to integrate Eqs. (15)–(17). Then we switched back to x as an independent variable to present results of this integration.

Following Ref. [10], we have used the dimensionless parameter $\alpha_f = 8\pi n_0 m_p c^2 \sqrt{\Gamma_0^2 - 1} / B_f^2$ as a measure of the beam density instead of α . The parameter α_f is more convenient than α for integration of Eqs. (15)–(17) because such integration is performed from $x=0$ to $x=x_p$. In our calculations the value of α_f varies in a wide range from 10^{-2} to 10^3 .

To integrate Eq. (16), the following two kinds of boundary condition for E_x were specified: $E_x|_{x=0}=0$ or $E_x|_{x=x_p}=0$. Integration of Eq. (16) for the boundary condi-

TABLE IV. Parameters of simulations of stationary collision between the beam with $\Gamma_0=300$ and the magnetic barrier for the boundary condition $E_x|_{x=x_p}=0$.

Run	α_f	α	$\frac{\Gamma_{p,\min}}{\Gamma_0}$	$\frac{\Gamma_{e,\max}}{\Gamma_0}$	$\frac{B_f}{B_0}$	$\frac{E_f}{B_0}$	$\frac{E_{\max}}{B_0}$
SR1	0.01	0.0098	0.99	1.02	0.99	-0.015	-0.015
SR2	1/10	0.086	0.92	1.2	0.92	-0.13	-0.13
SR3	1/5	0.15	0.86	1.3	0.87	-0.22	-0.22
SR4	1/2	0.29	0.76	2.1	0.76	-0.40	-0.41
SR5	1	0.44	0.67	7.1	0.67	-0.57	-0.58
SR6	2	0.50	0.64	48	0.50	-0.50	-0.62
SR7	4	0.51	0.64	97	0.36	-0.38	-0.61
SR8	10	0.51	0.63	170	0.23	-0.27	-0.58
SR9	40	0.51	0.63	276	0.11	-0.20	-0.53
SR10	1000	0.51	0.62	434	0.023	-0.14	-0.45

TABLE V. Parameters of simulations of stationary collision between the beam with $\Gamma_0=300$ and the magnetic barrier for the boundary condition $E_x|_{x=0}=0$.

Run	α_f	α	$\frac{\Gamma_{p,\max}}{\Gamma_0}$	$\frac{B_f}{B_0}$	$\frac{E_x(x_p)}{B_0}$
SL1	0.01	9.8×10^{-3}	1	0.99	0.016
SL2	1/10	0.082	1.06	0.90	0.15
SL3	1/5	0.13	1.1	0.81	0.29
SL4	1/3	0.16	1.3	0.69	0.45
SL5	1/2	0.15	1.5	0.55	0.63
SL6	2/3	0.11	1.9	0.41	0.78
SL7	3/4	0.085	2.2	0.34	0.85
SL8	0.8	0.068	2.5	0.29	0.88
SL9	0.9	0.032	3.7	0.19	0.95
SL10	1	4.6×10^{-4}	31	0.02	1

tion $E_x|_{x=x_p}=0$ was carried out with a ‘‘shooting method’’ technique. The electric field was guessed at the left boundary $x=0$ and Eq. (16) was integrated with all the quantities specified on that boundary. Then the electric field on the left boundary was adjusted to give a closer agreement with the boundary condition $E_x|_{x=x_p}=0$. Such shots were repeated until the boundary condition for the electric field was satisfied with a desirable accuracy. As a rule, only a few shots were required to reach the accuracy of $\sim 1\%$.

The computational engine we used to solve the regularized set of equations was the LSODE package [15] together with the OCTAVE interpreter [16]. The developed octave script is mostly compatible with the popular MATLAB [17] language.

Figure 9 shows typical numerical solutions for the longitudinal electric field E_x , the magnetic field B_z , and the x component of the four-velocity of electrons $u_{e,x}$ in run SR10. In this run, the boundary condition for E_x is $E_x|_{x=x_p}=0$. The energies of both electrons and protons inside the barrier are shown in Fig. 10. The results of our calculations are summarized in Tables IV and V. From these tables and Fig. 9 we can see that the electric field E_x is not equal to zero at $x=0$ and $x=x_p$ at once, as mentioned above. A common feature of all stationary solutions is that the electric and magnetic fields sharply increase near the electron turning point x_e as it was pointed out in Ref. [10]. There is the following tendency: The greater the value of α_f , the sharper the rise of the fields. Due to the change of independent variables discussed above, the sharp rise of the fields at the electron turning point is well resolved: It covers a large number of integration points and derivatives of the fields with respect to the new independent variable remain finite (see Fig. 11). The latter facts allow us to claim a high accuracy of our calculations.

In the paper of Peter *et al.* [10], Eqs. (15)–(17) were integrated directly using x as an independent variable and therefore they ran into serious difficulties on their way [18], which led to certain mistakes. For example, they were not able to calculate the value $E_x(x)$ at $x=x_e$ directly and the integration of Eq. (16) was treated as a two-point boundary value problem, adjusting $E_x(x_e)$ to be equal to zero at both boundaries $E_x(0)=E_x(x_p)=0$. Our calculations show that

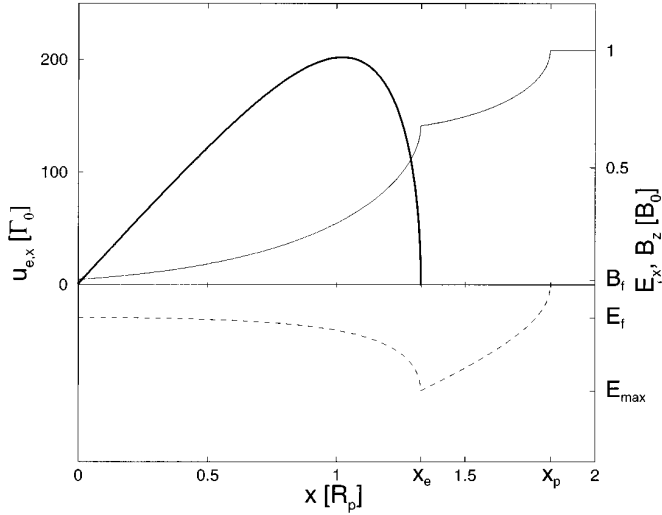


FIG. 9. Plots of the magnetic field $B_z(x)$ (thin solid line), the longitudinal electric field $E_x(x)$ (dotted line), and the x component of the four-velocity of electrons $u_{e,x}(x)$ (thick solid line) in run SR10.

such an adjustment is impossible (see Tables IV and V). The authors of Ref. [10] believed that at $\alpha_f \gg 1$ the orbit of electrons is strongly elongated in the y direction in a narrow vicinity of the electron turning point and the beam electrons move more or less along the barrier front with $x \approx x_e$ for a long time. As a result, a net charge in the collision region might be zero. We did not observe such a strong elongation of the electron orbit. Moreover, for the boundary condition $E_x|_{x=0}=0$ we have $\alpha_f \lesssim 1$, i.e., for this boundary condition α_f cannot be much more than unit.

We have confirmed the suggestion of Ref. [10] that electrons of the beam may be strongly accelerated inside the barrier. However, such an acceleration was observed only in runs with the boundary condition for E_x in the form $E_x|_{x=x_p}=0$. For the boundary condition $E_x|_{x=0}=0$, the beam electrons do not penetrate substantially deeper into the barrier than their gyroradius in the field B_f and their acceleration is very small.

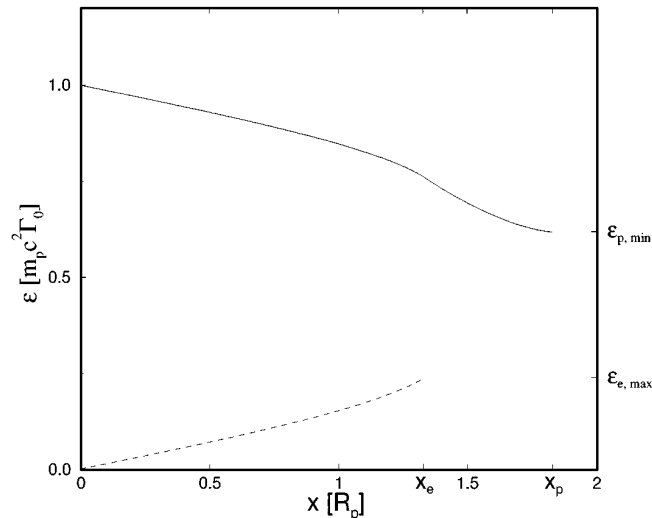


FIG. 10. Plots of the proton energy (solid line) and the electron energy (dotted line) in run SR10.

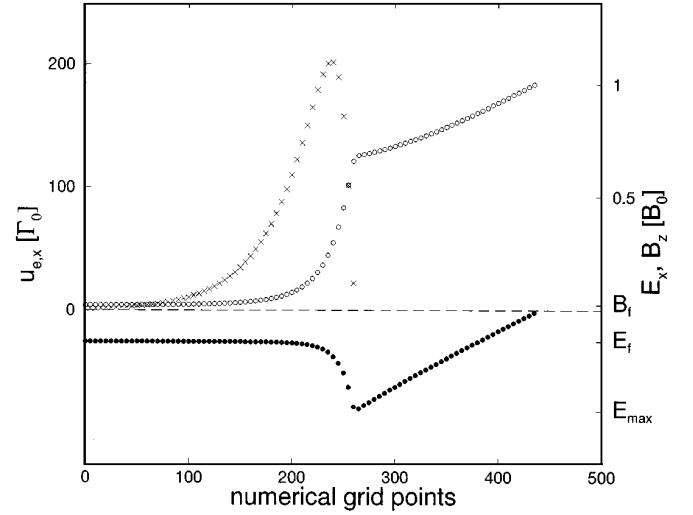


FIG. 11. Numerical resolution of the main results of the stationary case, run SR10. \circ , magnetic field profile; \bullet , electric field profile; \times , longitudinal component four-velocity of electrons. Each figure stands for five integration points.

For the boundary condition $E_x|_{x=x_p}=0$, a stationary solution of Eqs. (15)–(17) can exist for any nonzero value of α_f . For all these solutions, we have $\alpha \leq 0.5$ (see Fig. 12). This upper limit on α is more or less evident since in a stationary case the ram pressure of the beam cannot be more than the magnetic-field pressure of the barrier. As for the case of the boundary condition $E_x|_{x=0}=0$, a stationary solution can exist only if $\alpha_f \leq 1$ and $\alpha \leq 0.2$. This reduction of the upper limit on α occurs because in such a solution the electric field E_x far enough from the barrier front is directed inside the barrier, $E_x > 0$ at $x \geq$ a few times x_e . This field causes protons to penetrate even deeper into the barrier and to generate even stronger electric field. At $\alpha_f > 1$, at some distance from the barrier front the electric field inside the collision region is stronger than the magnetic field and the barrier cannot suppress penetration of protons inside itself.

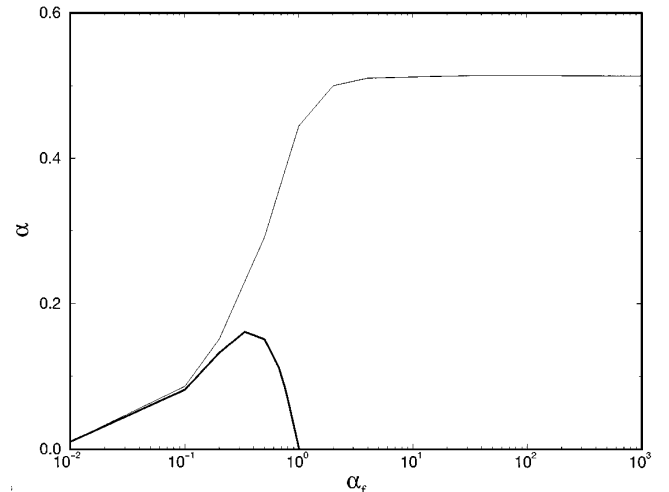


FIG. 12. Value of α as a function of α_f for both the boundary condition $E_x|_{x=x_p}=0$ (thin line) and the boundary condition $E_x|_{x=0}=0$ (thick line).

V. DISCUSSION

One of the main results of our time-dependent simulations presented in Sec. III is that the outflowing electrons are strongly accelerated near the barrier front and accumulate a substantial portion of the kinetic energy of protons. At $\alpha \sim 1$, when the ram pressure of the beam is equal to the magnetic-field pressure of the barrier, the fraction of the kinetic energy of protons that is transferred to outgoing electrons is up to $\sim 20\%$. The acceleration of outflowing electrons is completely due to nonstationarity of electromagnetic fields that are induced inside and near the barrier during the beam-barrier interaction. Indeed, in a stationary case the electric field is constant in time and depends on the x coordinate only, $\mathbf{E} = \{E_x(x), 0, 0\}$. If, as in both Ref. [10] and Sec. IV, the energy losses of electrons due to their radiation inside the barrier are ignored, the electron energy is a function of x only and the energy of reversed electrons outside the barrier coincides with their initial energy before the beam-barrier collision.

The bunching of reversed protons is a key element of nonstationarity of the beam-barrier collision. Roughly, the process of bunch formation may be illustrated in the following way. The first protons, which enter the barrier from $t = 0$ to $t \ll T_p$, run along an almost semicircular trajectory in an almost unperturbed field of the magnetic barrier. For the same Lorentz factor, the gyroradius of electrons is much smaller than the gyroradius of protons. Therefore, electrons cannot penetrate as deep as protons into the barrier. The separation of electric charges induce a strong electric field E_x in the x direction according to Eq. (1). The following protons “feel” this electric field. The field E_x decelerates protons and accelerates electrons. Protons that are injected into the barrier later run along “shorter” trajectories and spend less time inside the barrier. As a result, in about half of a proton gyroperiod, $t \sim \frac{1}{2}T_p$, most of the protons quit the barrier almost simultaneously and formation of the second bunch begins, and so on.

In the case of large α , the velocities v_x of reversed protons in the x direction are quite different (see Fig. 5) so that the bunches will decay at some distance from the barrier. Once there is no bunching at all in the low- α case, no bunches can be observed far from the barrier no matter what α is considered.

The propagation of plasma beams across a magnetic field is one of the oldest problems in plasma physics. In spite of the long history of investigation (e.g., Ref. [8]), a clear model of this phenomenon is yet to emerge. However, some general conclusions about the beam-magnetic-field interaction were made many years ago. For example, if the plasma flow pressure is more than the magnetic-field pressure, it is possible for the plasma to cross the field by purely magnetohydrodynamic principles. This propagation mode is equivalent to the motion of a solid conductor across the field. During propagation, the plasma beam picks up and carries along the ambient plasma and magnetic field. Such models of the beam propagation into the magnetic field are based on the diamagnetic properties of the plasma. Most probably, in our time-dependent simulations we observed such a propagation mode. Physically, the pushing of the magnetic field is provided by strong transverse electric currents (j_y) in the

domain $x_{\text{pen}}(t) - (c/\omega_{Bp}) < x < x_{\text{pen}}(t)$, where $x_{\text{pen}}(t)$ is the x coordinate of the most deeply penetrated particle. If α is large enough ($\alpha > \alpha_{\text{cr}}$), this current layer screens strongly the external magnetic field of the barrier at $x < x_{\text{pen}}(t) - (c/\omega_{Bp})$ and moves deeper and deeper into the barrier. From our time-dependent simulations, we have $\alpha_{\text{cr}} \approx 0.4$. This is more or less consistent with the conclusion that there are no stationary solutions for the beam-barrier collision if α is more than $\sim (0.2-0.5)$ depending on the boundary condition on the field E_x .

Many important features of our nonstationary solutions are absent in a stationary one. They are energy transfer from incoming protons to outgoing electrons, bunching of outgoing protons, excitation of low-frequency electromagnetic waves, etc.

The main question that still remains open is what the final state of the beam-barrier system in a very long-time run ($t \gg T_p$) is. As noted, we did not observe any decay of nonstationarity of the beam-barrier interaction, even in simulations extended up to $t_{\text{max}} \approx 16T_p$. However, it is possible that at ($t \gg 10T_p$) our nonstationary solution tends to a stationary one. It is worth noting that, in turn, a stationary solution of the beam-barrier collision might be unstable if α is high enough. Indeed, the energy of electrons inside the barrier may be a few hundred times higher than their initial energy. In this case, small ($\sim 10^{-2}$) perturbations might result in that some part of the reversed, $v_x < 0$, electrons is stopped and captured inside the barrier before reaching the barrier front. In addition, electrons may be captured by the barrier because of their energy losses via synchrotron emission in electric and magnetic fields if these fields are strong enough. In turn, such a capture of electrons may result in complete destruction of the stationary solution.

The beam-barrier collision is similar, in many respects, to collisionless shocks. Such shocks in astrophysical settings can and do accelerate charged particles to high energies (for a review see Refs. [19,20]). The efficiency of particle acceleration by shocks may be as high as $\sim 20-40\%$ (e.g., Ref. [19]). This value is more or less the same as the fraction of the kinetic energy of the beam that may be transferred to high-energy electrons in the process of the beam-barrier collision.

In addition to analytical calculations (e.g., Refs. [21,22]), acceleration of particles by shocks was studied numerically in both test particle Monte Carlo simulations (see Ref. [23] and references therein) and self-consistent plasma simulations (e.g., Refs. [24-27]). Most current self-consistent simulations of plasma shocks used in astrophysics are of the hybrid type because the m_e/m_p ratio is small, $m_e/m_p \approx 0.54 \times 10^{-3}$. In the hybrid approach, the ions are treated kinetically using standard particle-in-cell techniques, while the electrons are treated as a massless, charge neutralizing fluid. In our simulations we did not use the hybrid approach because the case of the ultrarelativistic beam is, in some respects, easier than the nonrelativistic case. This is because in our case, $\Gamma_0 \gg 1$, electrons are accelerated fast, and the mean energy becomes only an order of magnitude smaller than the mean energy of protons. In this case, the ratio of the gyroradii of electrons and protons is about two orders of magnitude larger than m_e/m_p , which is the ratio of the gyroradii of electrons and protons in nonrelativistic plasma.

This allowed us to treat both electrons and protons kinetically.

The configuration considered in our simulations is not quite self-consistent. Indeed, the barrier magnetic field has to be generated by some kind of current flowing in the plane $x=0$ in the y direction. However, the evolution of this current, because of its interaction with the induced electromagnetic fields, was not studied. In laboratory experiments, an external current flowing along a sheet of thin wires can be

the barrier-front current. As for a situation that is relevant for astrophysics, the barrier field has to be generated by the magnetized plasma of the barrier. Numerical considerations of such a configuration are under way.

ACKNOWLEDGMENTS

This research was supported by the MINERVA Foundation, Munich, Germany.

-
- [1] T. V. Cawthorne, in *Beams and Jets in Astrophysics*, edited by P. A. Hughes (Cambridge University Press, Cambridge, 1991), p. 187.
- [2] M. G. Baring, *Astrophys. J., Suppl. Ser.* **90**, 899 (1993).
- [3] R. Narayan, B. Paczyński, and T. Piran, *Astrophys. J.* **395**, L83 (1992).
- [4] V. V. Usov, *Nature (London)* **357**, 472 (1992).
- [5] V. V. Usov, *Mon. Not. R. Astron. Soc.* **267**, 1035 (1994).
- [6] C. Tompson and R. C. Duncan, *Astrophys. J.* **408**, 194 (1993).
- [7] P. Mészáros and M. J. Rees, *Astrophys. J.* **405**, 278 (1993).
- [8] K. Papadopoulos, A. Mankofsky, R. C. Davidson, and A. T. Drobot, *Phys. Fluids B* **3**, 1075 (1991); A. V. Gordeev, A. S. Kingsep, and L. I. Rudakov, *Phys. Rep.* **243**, 215 (1994).
- [9] M. N. Rosenbluth, in *Plasma Physics and Thermonuclear Research*, edited by C. L. Longmire, J. L. Tuck, and W. B. Thomson (Pergamon, New York, 1963), Vol. 2, p. 271.
- [10] W. Peter, A. Ron, and N. Rostocker, *Phys. Fluids* **22**, 1471 (1979).
- [11] M. V. Smol'sky and V. V. Usov, *Astrophys. J.* **461**, 858 (1996).
- [12] L. D. Landau and E. M. Lifshitz, *The Classical Theory of Fields* (Pergamon, New York, 1971).
- [13] G. B. Rybicki and A. P. Lightman, *Radiative Processes in Astrophysics* (Wiley, New York, 1979).
- [14] M. Hoshino, J. Arons, Y. A. Gallant, and A. B. Langdon, *Astrophys. J.* **390**, 454 (1992).
- [15] A collection of FORTRAN solvers for the initial value problem for ordinary differential equation systems, <http://www.netlib.org/odepack>.
- [16] OCTAVE, a high-level language, primarily intended for numerical computations, <http://www.che.wisc.edu/octave/>.
- [17] <http://www.mathworks.com/>.
- [18] W. Peter (private communication).
- [19] R. D. Blandford and D. Eichler, *Phys. Rep.* **154**, 1 (1987).
- [20] F. C. Jones and D. C. Ellison, *Space Sci. Rev.* **58**, 259 (1991).
- [21] J. R. Jokipii, *Astrophys. J.* **313**, 842 (1987).
- [22] M. Ostrowski, *Mon. Not. R. Astron. Soc.* **233**, 257 (1988).
- [23] M. G. Baring, D. C. Ellison, and F. C. Jones, *Adv. Space Sci.* **8/9**, 397 (1995).
- [24] K. Guest, *J. Geophys. Res.* **93**, 9649 (1988).
- [25] D. Burgess, *Geophys. Res. Lett.* **16**, 345 (1989).
- [26] M. Scholer, *Geophys. Res. Lett.* **17**, 1821 (1990).
- [27] D. Krauss-Varban and D. Burgess, *J. Geophys. Res.* **96**, 143 (1991).